Electronic Supplementary Material (ESI) for Physical Chemistry Chemical Physics.
This journal is © the Owner Societies 2023

Supporting Information

Correlation of Spin State and Catalytic Property of M-N_4 Single-Atom Catalyst in Oxygen Reduction Reaction

Wei Zhang,[1#] Jin-kong Pan,[#1,2] Yi-fan Yu,[1] Xian-jie Zhang,[1] Jia-hao Wang,[1] Wen-xian Chen,[1] Gui-lin Zhuang*[1]

[1]Institute of Industrial Catalysis, State Key Laboratory Breeding Base of Green-Chemical Synthesis Technology, College of Chemical Engineering, Zhejiang University of Technology, Hangzhou 310032, P.R. China.

[2]Wanbangde Pharmaceutical Group Co., Ltd.

[#] They contribute equally to this manuscript.

glzhuang@zjut.edu.cn (G. L. Zhuang)

Table of contents

Computational Details

Linear Response Calculation for the effective U_{eff} parameters: The U_{eff} parameters of Mn (II), Fe (II) and Co (II) were evaluated by Quantum ESPRESSO 7.1 package[1] using the linear response approach introduced by Cococcioni et.al[2]. In this calculation, Perdew, Burke and Ernzerhof (PBE)[3] function was utilized to treat the exchange-correlation interaction, and the Vanderbilt ultrasoft pseudopotentials[4] was used to expand the plane-wave function under the energy cutoff of 40 Ryd and kinetic energy cutoff of 450 Ryd for charge density and potential. The convergence threshold for self-consistency was set to 10^{-9} and the 8×8×1 Monkhorst-Pack grid[5] was employed in the sampling of Brillouin zone. Based on invariant formulation, the total energy for DFT + U can be typically described as follows:

$$E_{DFT+U}[n(r)] = E_{DFT}[n(r)] + E_U\left[\left\{n^{I\sigma}_{mm'}\right\}\right] \quad \text{(eq 1)}$$

Where, E_{DFT} is a total energy from noninteraction Kohn-Sham algorithm; E_U is Hubbard correction. Furthermore, if neglecting higher-multipolar terms of Coulomb interaction, E_U is written as:

$$E_U\left[\left\{n^{I\sigma}_{mn_i}\right\}\right] = \frac{U-J}{2}\sum_{I,\sigma}\mathrm{Tr}\left[n^{I\sigma}\left(1-n^{I\sigma}\right)\right] = \frac{U_{eff}}{2}\sum_{I,\sigma}\mathrm{Tr}\left[n^{I\sigma}\left(1-n^{I\sigma}\right)\right] \quad \text{(eq 2)}$$

By linear-response approach U method, the linear response function is defined as

$$\chi = \frac{\partial n}{\partial \alpha} \quad \text{(eq 3)}$$

In this method, the interacting (χ) and noninteractiong density response functions with respect to localized perturbations were firstly calculated. Thus U can be obtained by following formula:

$$U_{eff} = \chi_1^{-1} - \chi_0^{-1} \quad \text{(eq 4)}$$

By changing the rigid potential shifts α, we obtain the bare and self-consistent occupation regression response functions. The interacting (χ_1) and the noninteracting (χ_0) are the slopes of bare and self-consistent regression response functions, respectively. Thus, the obtained U_{eff} parameters are 4.820 eV for Mn (**Figure S1**), 5.875 eV for Fe (**Figure S2**) and 5.382 eV for Co (**Figure S3**) ions.

Spin States of Cluster models M-N_4-C: These calculations were carried out utilizing the Gaussian 16 program[6]. The modified B3LYP hybrid functional (B3LYP*), where the amount of HF exchange was lowered to 15% from 20% in the standard B3LYP, and the pure functionals OPBE, based on the OPTX-based exchange functional, are regarded as the good description for the electronic states of transition metal (Mn, Fe, Co and et.al.) ions. Both double-zeta basis set with polarization functions (def2SVP) and triple-zeta basis set with polarization functions (def2TZVP) basis set are utilized to treat wave functions. The initial configurations derived from the optimized structure from VASP[7] were further saturated by hydrogen atoms, as shown in **Figure S4** and fully relaxed by def2SVP with two functional.

Free-Energy Computational Details: The free energy is calculated mainly according to the following formula: $\Delta G = \Delta E + \Delta E_{ZPE} - T\Delta S + \Delta G_U$, in which the calculations of *ZPE* and *S* are the key. *ZPE* was defined as $ZPE = \Sigma_i 1/2 h\nu_i$ (eq 5), where *i* was the frequency number, ν_i was the frequency with unit cm^{-1}. The adsorbed species were only taken vibrational entropy (S_v) into account, as shown in the following formula:

$$S_v = \sum_i R\left\{\frac{h\nu_i}{k_B T}\left[\exp\left(\frac{h\nu_i}{k_B T}\right)-1\right]^{-1} - \ln\left[1-\exp\left(-\frac{h\nu_i}{k_B T}\right)\right]\right\} \quad \text{(eq 6)}$$

among which $R = 8.314\ J\cdot mol^{-1}\cdot K^{-1}$, $T = 298.15$ K, $h = 6.63 \times 10^{-34}\ J\cdot s$, $k_B = 1.38 \times 10^{-23}\ J\cdot K^{-1}$, where *i* was the frequency number, ν_i was the frequency with unit cm^{-1}. In calculation process of frequency, M-N_4-C is fixed and adsorbed species are free for intermediates. For degrees of freedom, each free atom has 6 degrees of freedom (3 degrees of translational freedom and 3 degrees of rotational freedom).

Dependence Computation of Potential on Energy: The solvent environment was simulated by the VASPsol code.[8-10] The relative permittivity was set to 80 for applied model in aqueous electrolyte. The contribution of cavitation energy was ignored by setting TAU = 0 in VASPsol. The applied potential to the electrochemical interface was simulated by adding or removing electrons in the supercell (Δn: from -

2e to 2e in steps of 1e). The potential-dependent energy of the system (E) was calculated as following equation:[11-13]

$$E = E_{DFT} - \Delta n \left(V_{sol} + \Phi_q/e\right) \quad \text{(eq 7)}$$

where E_{DFT} is the energy directly obtained from DFT calculations, V_{sol} is the electrostatic potential of the bulk electrolyte, and Φ_q is the work function of the charged system. The relation between Φq and the corresponding electrode potential referenced to the standard hydrogen electrode (SHE) scale is formulated:

$$U_q(\text{V / SHE}) = -4.6\ \text{V} - \Phi_q/e \quad \text{(eq 8)}$$

where −4.6 V is the absolute electrode potential of the SHE benchmarked in VASPsol.

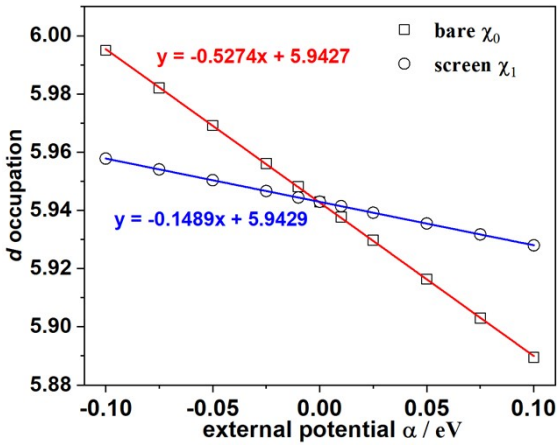

Figure S1. Interacting (χ_1) and noninteracting (χ_0) density response functions of Mn-N_4-C catalyst.

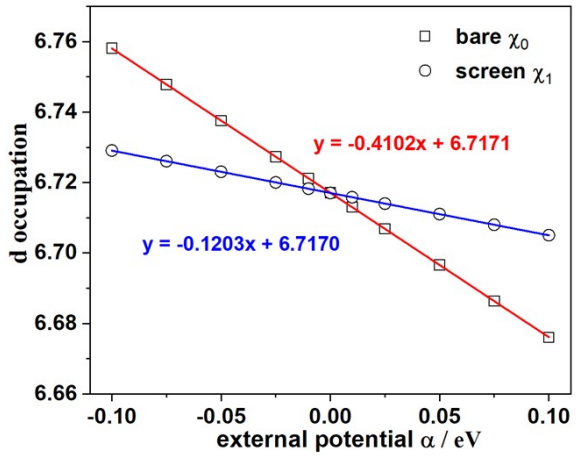

Figure S2. Interacting (χ_1) and noninteracting (χ_0) density response functions of Fe-N_4-C catalyst.

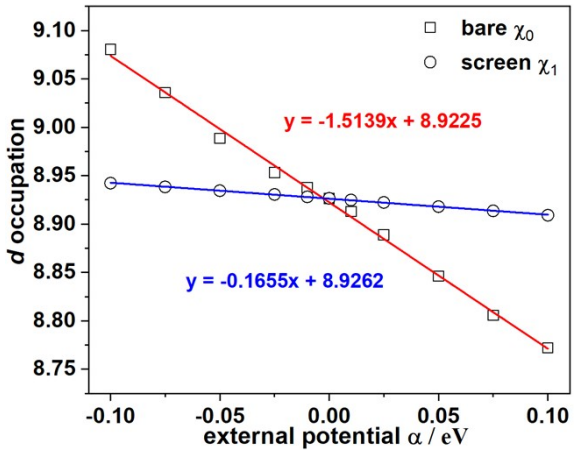

Figure S3. Interacting (χ_1) and noninteracting (χ_0) density response functions of Co-N_4-C catalyst.

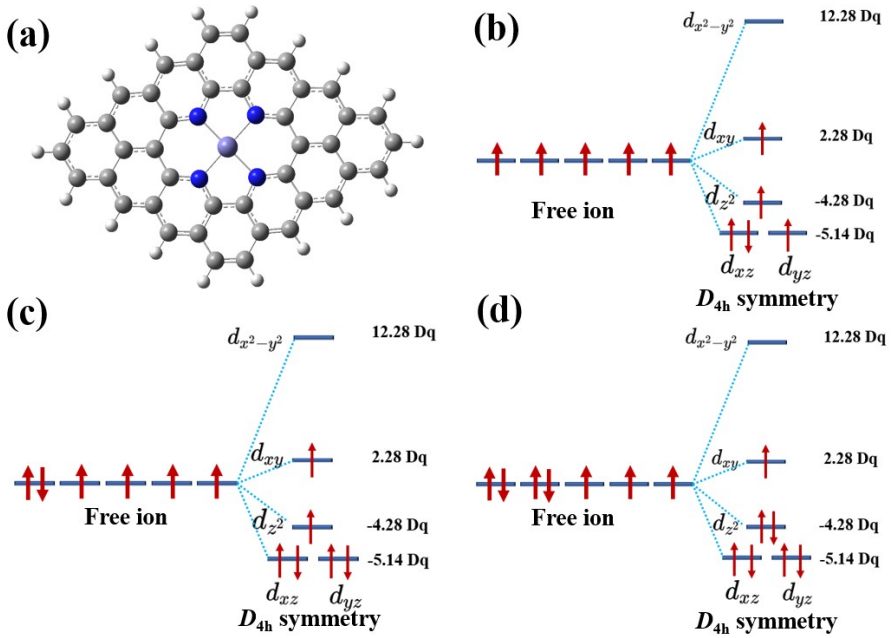

Figure S4. (a) The cluster model of M-N_4-C (M = Mn, Fe, Co) and *d*-block energy level splitting scheme of Mn (b), Fe (c) and Co (d) under D_{4h} symmetry square planar coordination.

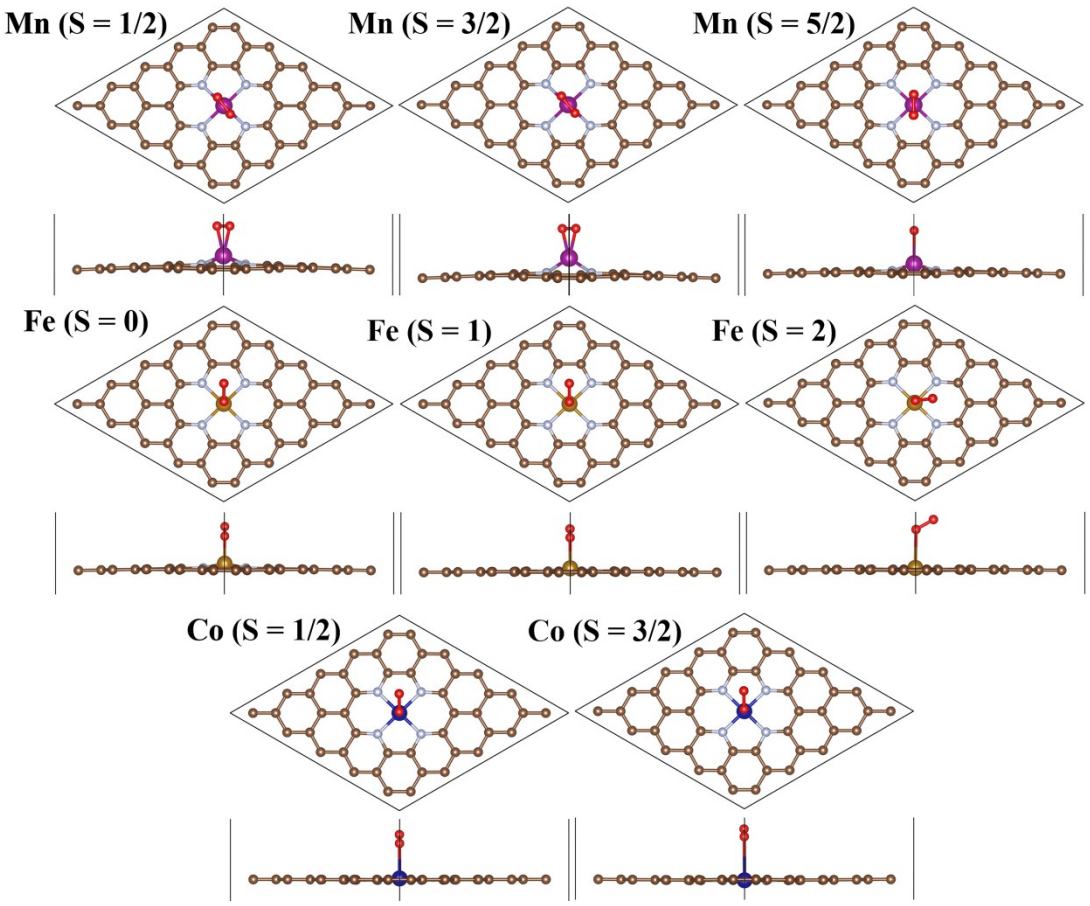

Figure S5. The optimized structures of M-N_4-C (M = Mn, Fe, Co) with adsorbed O_2.

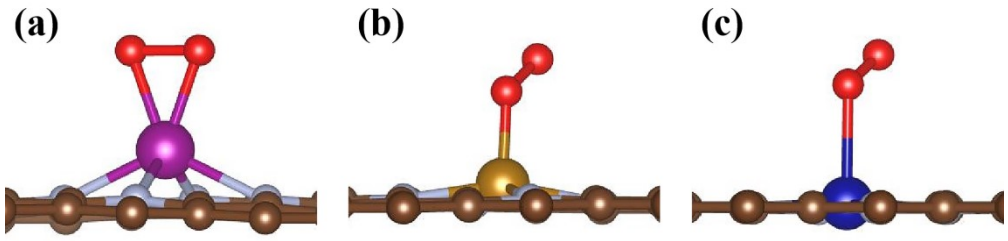

Figure S6. The most stable adsorption configuration of O_2 on Mn-N_4-C (S = 3/2), Fe-N_4-C (S = 0), Co-N_4-C (S = 1/2).

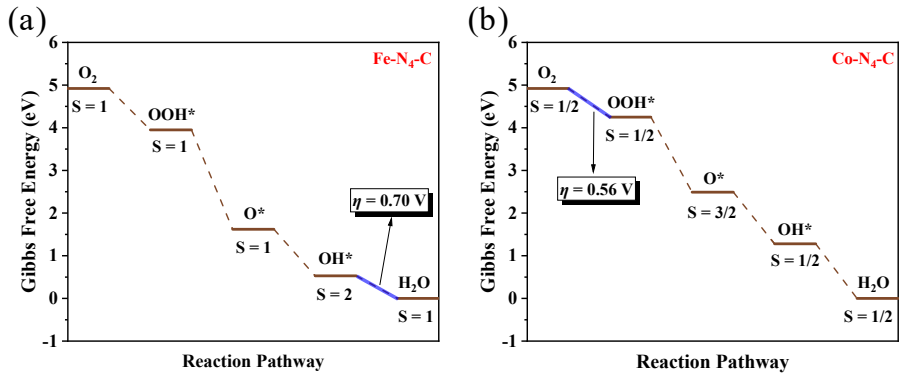

Figure S7. The free energy changes of 4e$^-$ ORR on (a) Fe-N_4-C and (b) Co-N_4-C via spin crossover.

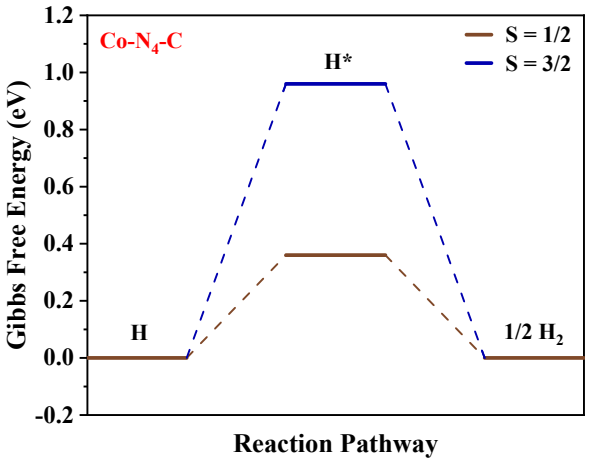

Figure S8. The free energy changes of HER on Co-N_4-C (S = 1/2, 3/2).

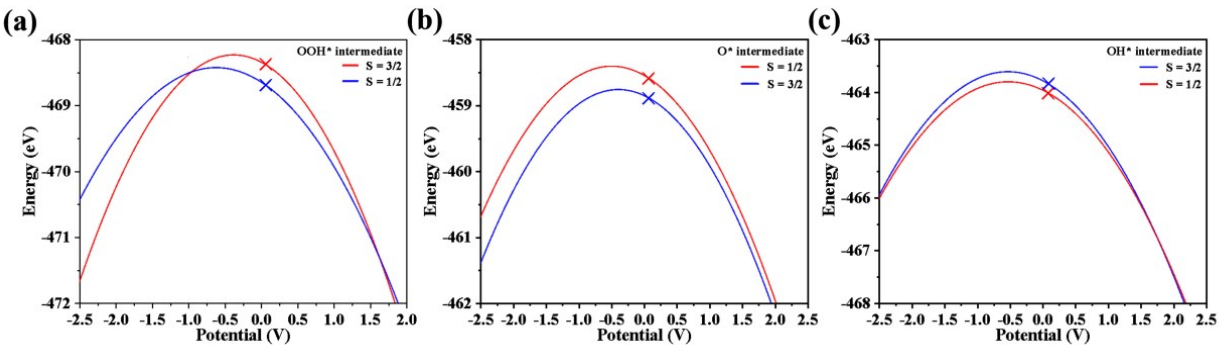

Figure S9. Schematics of three intermediates (OOH*, O*, OH*) involving spin-state transitions on Co-N_4-C (S = 1/2, 3/2) with outstanding 2e$^-$ ORR performance.

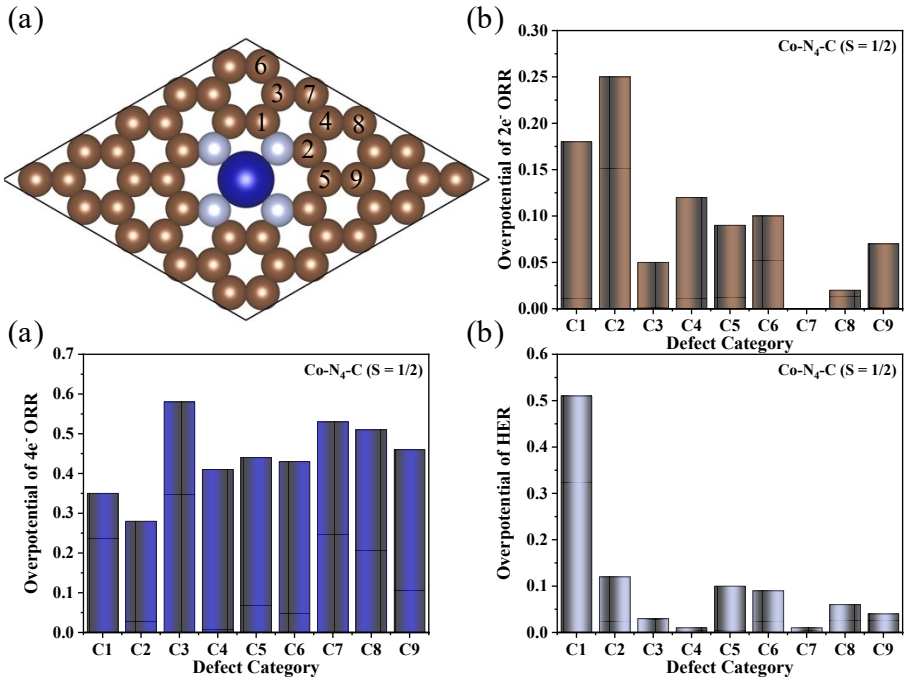

Figure S10. (a) The defect category (C1 - C9). The overpotentials of (b) 2e$^-$ ORR, (c) 4e$^-$ ORR and (d) HER on Co-N_4-C (S = 1/2) with C1-C9 defects.

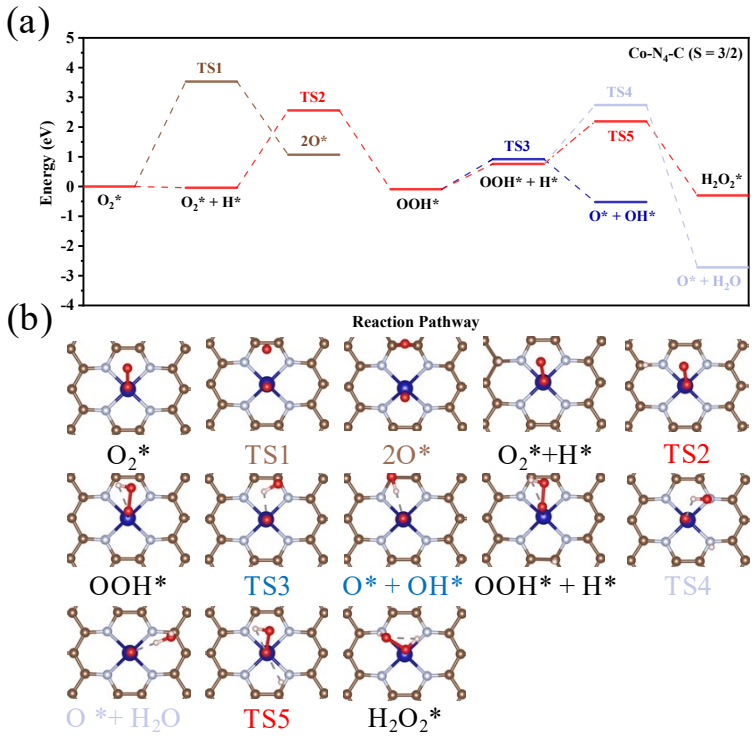

Figure S11. (a) The energy barrier diagram of ORR on Co-N_4-C (S = 3/2). (b) The structures of intermediates and transition state.

Table S1. The structure energies (eV) of M-N_4-C with different spin states of Mn, Fe, Co under U_{eff} values (eV) of 4.820 eV, 5.875 eV, 5.382 eV via PBE-U, OPBE and B3LYP* functions.

U_{eff} values	M-N_4-C	PBE-U	OPBE	B3LYP*
4.820	Mn (S = 1/2)	-444.51	-448.54	-487.63
	Mn (S = 3/2)	**-446.04**	**-449.49**	**-488.67**
	Mn (S = 5/2)	-445.93	-448.77	-487.73
5.875	Fe (S = 0)	-442.85	-446.97	-486.86
	Fe (S = 1)	-444.67	**-447.88**	**-487.40**
	Fe (S = 2)	**-444.77**	-447.07	-486.46
5.382	Co (S = 1/2)	**-443.70**	**-446.60**	**-485.65**
	Co (S = 3/2)	-443.41	-445.52	-484.61

Table S2. The structure energies (eV) of Fe-N_4-C with different spin states of Fe under U_{eff} values (eV) of 3.1 eV via PBE-U, OPBE and B3LYP* functions.

U_{eff} values	M-N_4-C	PBE-U	OPBE	B3LYP*
3.1	Fe (S = 0)	-444.78	-446.96	-486.83
	Fe (S = 1)	**-445.52**	**-447.92**	**-487.40**
	Fe (S = 2)	-444.28	-447.07	-486.49

Table S3. The magnetic moments (μ_B) of M in M-N_4-C (M = Mn, Fe, Co) via PBE-U, OPBE and B3LYP* functions.

M-N_4-C	PBE-U	OPBE	B3LPY*
Mn (S = 1/2)	1.05	2.98	1.09
Mn (S = 3/2)	3.22	3.16	2.99
Mn (S = 5/2)	4.42	3.90	4.15
Fe (S = 0)	-0.15	0.00	0.00
Fe (S = 1)	2.04	1.98	1.90
Fe (S = 2)	2.50	3.38	3.51
Co (S = 1/2)	1.04	0.77	0.94
Co (S = 3/2)	2.69	1.20	2.57

Table S4. The M-N bond length (Å) on M-N_4-C (M = Mn, Fe, Co with different spin states).

M-N_4-C	M-N1	M-N2	M-N3	M-N4	Average
Mn (S = 1/2)	1.93	1.93	1.93	1.93	1.93
Mn (S = 3/2)	1.92	1.92	1.92	1.92	1.92
Mn (S = 5/2)	1.98	1.98	1.98	1.98	1.98
Fe (S = 0)	1.90	1.90	1.90	1.90	1.90
Fe (S = 1)	1.91	1.91	1.91	1.91	1.91
Fe (S = 2)	1.96	1.96	1.96	1.96	1.96
Co (S = 1/2)	1.90	1.90	1.90	1.90	1.90
Co (S = 3/2)	1.94	1.94	1.94	1.94	1.94

Table S5. The relative energies (kcal/mol) and Mn magnetic moments (μ_B) for Mn-N_4-C with different spin states under the two different functions (B3LYP* and OPBE) and basis sets (def2SVP and def2TZVP)[a].

Spin State	B3LYP*		OPBE	
	Energy	**Mag. Mom.**	**Energy**	**Mag. Mom.**
		def2SVP		
1/2	18.252	1.056	33.084	3.462
3/2	0.000	3.258	0.000	3.619
5/2	1.616	3.393	0.565	3.797
		def2TZVP		
1/2	20.550	1.049	32.578	3.601
3/2	0.000	3.292	0.000	3.716
5/2	1.697	3.375	0.753	3.920

a：The structures in def2TZVP is derived from the optimization using def2SVP.

Table S6. The relative energies (kcal/mol) and Fe magnetic moments (μ_B) for Fe-N_4-C with different spin states under the two different functions (B3LYP* and OPBE) and basis sets (def2SVP and def2TZVP)[a].

Spin State	B3LYP*		OPBE	
	Energy	**Mag. Mom.**	**Energy**	**Mag. Mom.**
		def2SVP		
0	36.226	0.650	39.169	0.000
1	0.000	2.001	0.000	2.222
2	2.479	2.010	3.600	2.272
		def2TZVP		
0	34.085	0.087	15.212	0.000
1	0.000	2.053	0.000	2.288
2	2.895	2.054	3.380	2.306

a：The structures in def2TZVP is derived from the optimization using def2SVP.

Table S7. The relative energies (kcal/mol) and Co magnetic moments (μ_B) for Co-N_4-C with different spin states under the two different functions (B3LYP* and OPBE) and basis sets (def2SVP and def2TZVP)[a].

Spin State	B3LYP*		OPBE	
	Energy	**Mag. Mom.**	**Energy**	**Mag. Mom.**
		def2SVP		
1/2	0.000	1.032	0.000	1.033
3/2	1.766	1.041	3.704	1.043
		def2TZVP		
1/2	0.000	1.050	0.000	1.064
3/2	1.948	1.053	3.446	1.053

a：The structures in def2TZVP is derived from the optimization using def2SVP.

Table S8. The adsorption energy (E_{ads}, eV) and the number of electron transfer between M-N_4-C (M = Mn, Fe, Co with different spin states) and O_2 molecule.

M-N_4-C	E_{ads}	Electron transfer
Mn (S = 1/2)	-0.11	0.61
Mn (S = 3/2)	-0.57	0.69
Mn (S = 5/2)	-0.33	0.61
Fe (S = 0)	-0.59	0.47
Fe (S = 1)	-0.23	0.44
Fe (S = 2)	-0.21	0.26
Co (S = 1/2)	-0.42	0.33
Co (S = 3/2)	-0.30	0.16

Table S9. The spin quantum numbers with spin selection rules and DFT-U//OPBE calculation for pristine M-N_4-C and M-N_4-C with adsorbed O_2.

	Mn-N_4-C		**Fe-N_4-C**		**Co-N_4-C**	
S_{MN4C}	3/2		1		1/2	
$S_{o2-MN4C}^{SSR}$	5/2, 3/2, 1/2		2, 1, 0		3/2, 1/2	
$S_{o2-MN4C}^{Cal}$	3/2		0		1/2	
	1/2	0.46	0	0.00	1/2	0.00
ΔE / eV	3/2	0.00	1	0.37	3/2	0.13
	5/2	0.24	2	0.38	/	/

Table S10. The free energy changes (eV) and overpotentials (V) of $4e^-$ ORR on M-N_4-C (M = Mn, Fe, Co with different spin states).

M-N_4-C	**$\Delta G1$**	**$\Delta G2$**	**$\Delta G3$**	**$\Delta G4$**	**overpotential**
Mn (S = 1/2)	-1.31	-2.72	-0.45	-0.43	0.80
Mn (S = 3/2)	-0.91	-2.23	-1.18	-0.60	0.63
Mn (S = 5/2)	-1.46	-1.53	-1.87	-0.06	1.17
Fe (S = 0)	-1.79	-1.79	-1.24	-0.11	1.12
Fe (S = 1)	-0.97	-2.33	-0.73	-0.89	0.50
Fe (S = 2)	-1.82	-2.01	-1.41	0.32	1.55
Co (S = 1/2)	-0.67	-1.45	-1.52	-1.28	0.56
Co (S = 3/2)	-1.19	-2.32	-0.95	-0.46	0.77

Table S11. The free energy changes (eV) of overpotentials (V) of $2e^-$ ORR on M-N_4-C (M = Mn, Fe, Co with different spin states).

M-N_4-C	$\Delta G1$	$\Delta G2$	overpotential
Mn (S = 1/2)	-1.31	-0.09	0.61
Mn (S = 3/2)	-0.91	-0.49	0.21
Mn (S = 5/2)	-1.46	0.06	0.76
Fe (S = 0)	-1.79	0.39	1.09
Fe (S = 1)	-0.97	-0.43	0.27
Fe (S = 2)	-1.82	0.42	1.12
Co (S = 1/2)	-0.67	-0.73	0.03
Co (S = 3/2)	-1.19	-0.21	0.49

Table S12. The energies (eV) of intermediates (O_2*, OOH*, O*, OH*).

M-N_4-C	E_{O2*}	E_{OOH*}	E_{O*}	E_{OH*}
Mn (S = 1/2)	-459.46	-463.40	-455.04	-459.17
Mn (S = 3/2)	-459.92	-463.96	-455.07	-459.90
Mn (S = 5/2)	-459.68	-463.77	-454.24	-459.69
Fe (S = 0)	-458.37	-462.26	-453.01	-457.90
Fe (S = 1)	-458.01	-462.40	-453.68	-458.03
Fe (S = 2)	-457.99	-462.37	-453.33	-458.40
Co (S = 1/2)	-456.88	-460.81	-451.19	-456.31
Co (S = 3/2)	-456.75	-460.23	-451.49	-456.09

Table S13. The free energy changes (eV) of overpotentials (V) of HER on Co-N_4-C (S = 1/2, 3/2).

M-N_4-C	ΔG1	ΔG2	overpotential
Co (S = 1/2)	0.36	-0.36	0.36
Co (S = 3/2)	0.96	-0.96	0.96

Table S14. Computed zero-point energy (*ZPE*, eV), entropy correction (*TS*, eV) on catalyst surfaces. The temperature is set to 298.15 K. The unit of data is eV.

Intermediate	M-N_4-C	*ZPE*	*TS*
OOH*	Mn (S = 1/2)	0.44	0.19
	Mn (S = 3/2)	0.42	0.16
	Mn (S = 5/2)	0.42	0.18
	Fe (S = 0)	0.43	0.21
	Fe (S = 1)	0.42	0.21
	Fe (S = 2)	0.42	0.23
	Co (S = 1/2)	0.43	0.19
	Co (S = 3/2)	0.43	0.21
O*	Mn (S = 1/2)	0.06	0.08
	Mn (S = 3/2)	0.05	0.10
	Mn (S = 5/2)	0.05	0.05
	Fe (S = 0)	0.07	0.07
	Fe (S = 1)	0.06	0.08
	Fe (S = 2)	0.06	0.10
	Co (S = 1/2)	0.06	0.07
	Co (S = 3/2)	0.06	0.08
OH*	Mn (S = 1/2)	0.34	0.08
	Mn (S = 3/2)	0.32	0.13
	Mn (S = 5/2)	0.32	0.15
	Fe (S = 0)	0.34	0.11

H*	Fe (S = 1)	0.33	0.13
	Fe (S = 2)	0.33	0.13
	Co (S = 1/2)	0.32	0.14
	Co (S = 3/2)	0.31	0.09
	Co (S = 1/2)	0.21	0.01
	Co (S = 3/2)	0.13	0.04

Table S15. The free energy changes (eV) of overpotentials (V) of $2e^-$ ORR on Co-N_4-C (S = 1/2) with nine types of individual C defects.

CX	**Δ*G*1**	**Δ*G*2**	**overpotential**
C1	-0.88	-0.52	0.18
C2	-0.95	-0.45	0.25
C3	-0.65	-0.75	0.05
C4	-0.82	-0.58	0.12
C5	-0.79	-0.61	0.09
C6	-0.80	-0.60	0.10
C7	-0.70	-0.70	0.00
C8	-0.72	-0.68	0.02
C9	-0.77	-0.63	0.07

Table S16. The free energy changes (eV) of overpotentials (V) of $4e^-$ ORR on Co-N_4-C (S = 1/2) with nine types of individual C defects.

CX	Δ*G*1	Δ*G*2	Δ*G*3	Δ*G*4	overpotential
C1	-0.88	-1.25	-1.86	-0.93	0.35
C2	-0.95	-1.50	-1.45	-1.02	0.28
C3	-0.65	-1.85	-1.41	-1.01	0.58
C4	-0.82	-1.76	-1.03	-1.30	0.41
C5	-0.79	-1.82	-1.38	-0.94	0.44
C6	-0.80	-1.48	-1.45	-1.19	0.43
C7	-0.70	-0.75	-2.21	-1.26	0.53
C8	-0.72	-1.49	-1.63	-1.07	0.51
C9	-0.77	-1.42	-1.42	-1.31	0.46

Table S17. The free energy changes (eV) of overpotentials (V) of HER on Co-N_4-C (S = 1/2) with nine types of individual C defects.

CX	Δ*G*1	Δ*G*2	overpotential
C1	0.51	-0.51	0.51
C2	0.12	-0.12	0.12
C3	-0.03	0.03	0.03
C4	-0.01	0.01	0.01
C5	-0.10	0.10	0.10
C6	0.09	-0.09	0.09
C7	0.01	-0.01	0.01
C8	0.06	-0.06	0.06
C9	0.04	-0.04	0.04

Table S18. The energy barrier (E_a, eV) for each elementary step of ORR on Co-N_4-C (S = 1/2).

Reaction pathway	E_a
O_2* → 2O*	4.03
O_2* + H* → OOH*	0.17
OOH* → O* + OH*	1.76
OOH* + H* → H_2O_2*	1.20
H_2O_2* → * + H_2O_2	0.07
OOH* + H* → O* + H_2O	1.26
H_2O_2* → 2OH*	0.58
H_2O_2* + H* → OH* + H_2O	1.60

Table S19. The energy barrier (E_a, eV) for each elementary step of ORR on Co-N_4-C (S = 3/2).

Reaction pathway	E_a
O_2* → 2O*	3.53
O_2* + H* → OOH*	2.60
OOH* → O* + OH*	1.01
OOH* + H* → H_2O_2*	1.43
OOH* + H* → O* + H_2O	1.97

Table S20. The number of electron transfer between Co-N_4-C (S = 1/2, 3/2) and adsorbed species (O_2, OOH, O, OH) and the spin state of intermediates.

Adsorbed specie	Spin state of Co-N_4-C	Spin state of intermediate	Electron transfer
O_2	1/2	1/2	0.33
	3/2	3/2	0.16
OOH	1/2	0	0.49
	3/2	1	0.58
O	1/2	0	0.61
	3/2	1	0.78
OH	1/2	0	0.51
	3/2	1	0.62

Table S21. The ICOHP of Co-O in Co-N_4-C (S = 1/2, 3/2) with adsorbed O_2 and OOH.

Spin	O_2*			OOH*		
state	spin1	spin2	average	spin1	spin2	average
1/2	-0.58	-0.73	-0.66	-0.53	-1.55	-1.04
3/2	-0.11	-0.17	-0.14	-0.97	-1.55	-1.26

Table S22. The ΔG_{OOH*} (eV), overpotentials (η, V) of 4e$^-$ ORR, the number of transferred electrons (N, e) from M-N_4-C to OOH, magnetic moment (MM, μ_B) of M in M-N_4-C with and without adsorbed OOH.

M-N_4-C	ΔG_{OOH*}	η	N	MM of M in OOH*	MM of M
Mn (S = 1/2)	3.61	0.80	0.46	0.00	1.05
Mn (S = 3/2)	4.01	0.63	0.57	3.66	3.22
Mn (S = 5/2)	3.46	1.17	0.62	4.40	4.42
Fe (S = 0)	3.13	1.12	0.41	1.14	-0.15
Fe (S = 1)	3.95	0.50	0.46	1.44	2.04
Fe (S = 2)	3.10	1.55	0.61	3.30	2.50
Co (S = 1/2)	4.25	0.56	0.49	0.00	1.04
Co (S = 3/2)	3.73	0.77	0.58	2.57	2.69

Table S23. The magnetic moment (μ_B) of Co in Co-N_4-C (S = 1/2) with adseobed O_2, OOH, O, OH due to outstanding 2e$^-$ ORR performance via PBE-U and OPBE functions.

intermediate	Spin state of M	PBE-U	OPBE
O_2*	1	0.08	-0.23
OOH*	0	0.00	0.00
O*	0	-0.04	0.00
OH*	0	0.00	0.00

REFERENCES

1. S. B. P. Giannozzi, N. Bonini, M. Calandra, *J. Phys-Condens. Mat*, 2009, **21**, 395502.
2. M. Cococcioni and S. de Gironcoli, *Phys. Rev. B*, 2005, **71**, 035105.
3. J. P. B. Perdew, K.; Ernzerhof, M, *Phys. Rev. Lett*, 1996, **77**, 3865-3868.
4. D. Vanderbilt, *Phys Rev B Condens Mat*, 1990, **41**, 7892-7895.
5. H. J. Monkhorst and J. D. Pack, *Phys Rev B*, 1976, **13**, 5188-5192.
6. M. J. Frisch, G. W. Trucks, H. B. Schlegel, G. E. Scuseria, M. A. Robb, J. R. Cheeseman, G. Scalmani, V. Barone, G. A. Petersson, H. Nakatsuji, X. Li, M. Caricato, A. V. Marenich, J. Bloino, B. G. Janesko, R. Gomperts, B. Mennucci, H. P. Hratchian, J. V. Ortiz, A. F. Izmaylov, J. L. Sonnenberg, Williams, F. Ding, F. Lipparini, F. Egidi, J. Goings, B. Peng, A. Petrone, T. Henderson, D. Ranasinghe, V. G. Zakrzewski, J. Gao, N. Rega, G. Zheng, W. Liang, M. Hada, M. Ehara, K. Toyota, R. Fukuda, J. Hasegawa, M. Ishida, T. Nakajima, Y. Honda, O. Kitao, H. Nakai, T. Vreven, K. Throssell, J. A. Montgomery Jr., J. E. Peralta, F. Ogliaro, M. J. Bearpark, J. J. Heyd, E. N. Brothers, K. N. Kudin, V. N. Staroverov, T. A. Keith, R. Kobayashi, J. Normand, K. Raghavachari, A. P. Rendell, J. C. Burant, S. S. Iyengar, J. Tomasi, M. Cossi, J. M. Millam, M. Klene, C. Adamo, R. Cammi, J. W. Ochterski, R. L. Martin, K. Morokuma, O. Farkas, J. B. Foresman and D. J. Fox, Wallingford, CT2016.
7. G. F. Kresse, J, *Phys. Rev. B*, 1996, **54**, 11169-11186.
8. K. Mathew, V. S. C. Kolluru, S. Mula, S. N. Steinmann and R. G. Hennig, *J Chem Phys*, 2019, **151**, 234101.
9. K. Mathew, R. Sundararaman, K. Letchworth-Weaver, T. A. Arias and R. G. Hennig, *J Chem Phys*, 2014, **140**, 084106-084114.
10. M. Fishman, H. L. Zhuang, K. Mathew, W. Dirschka and R. G. Hennig, *Phys. Rev. B*, 2013, **87**.
11. J. S. Filhol and M. Neurock, *Angew Chem Int Ed Engl*, 2006, **45**, 402-406.
12. Z. Duan and G. Henkelman, *ACS Catal*, 2020, **10**, 12148-12155.
13. X. Hu, S. Chen, L. Chen, Y. Tian, S. Yao, Z. Lu, X. Zhang and Z. Zhou, *J Am Chem Soc*, 2022, **144**, 18144-18152.